Original Article

Sustained Exposure to High Glucose Concentrations Modifies Glucose Signaling and the Mechanics of Secretory Vesicle Fusion in Primary Rat Pancreatic β-Cells

Takashi Tsuboi, Magalie A. Ravier, Laura E. Parton, and Guy A. Rutter

The mechanism(s) by which chronic hyperglycemia impairs glucose-stimulated insulin secretion is poorly defined. Here, we compare the "nanomechanics" of single exocytotic events in primary rat pancreatic β-cells cultured for 48 h at optimal (10 mmol/l) or elevated (30 mmol/l) glucose concentrations. Cargo release was imaged by total internal reflection fluorescence microscopy of lumen-targeted probes (neuropeptide Y [NPY]-pH–insensitive yellow fluorescent protein [NPY-Venus] or NPY–monomeric red fluorescent protein), while the fate of the vesicle membrane was reported simultaneously with phosphatase-on-the-granule-of-insulinoma–enhanced green fluorescent protein. Under all conditions studied, exocytosis proceeded via a "cavity recapture" mechanism in which the vesicle and plasma membranes fused transiently. While essentially complete release of NPY-Venus was observed in 24 ± 1% of glucose-stimulated exocytotic events in cells maintained at 10 mmol/l glucose, this value was reduced reversibly to 5 ± 2% of events by culture at 30 mmol/l glucose, in line with decreases in Glut2 and glucokinase gene expression, and attenuated glucose-stimulated increases in NADPH and intracellular [Ca^{2+}]. Since vesicle release in response to cell depolarization with KCl was not affected by culture at 30 mmol/l glucose, we conclude that hyperglycemia causes the abnormal termination of individual insulin release events principally by inhibiting glucose signaling. *Diabetes* 55:1057–1065, 2006

From the Department of Biochemistry, Henry Wellcome Laboratories for Integrated Cell Signalling, School of Medical Sciences, University Walk, University of Bristol, Bristol, U.K.

Address correspondence and reprint requests to Professor Guy A. Rutter, Department of Biochemistry, School of Medical Sciences, University of Bristol, University Walk, Bristol, BS8 1TD, U.K. E-mail: g.a.rutter@bristol.ac.uk.

Received for publication 6 December 2005 and accepted in revised form 17 January 2006.

T.T. and M.A.R. contributed equally to this study.

Additional information on this article can be found in an online appendix at http://diabetes.diabetesjournals.org.

[Ca^{2+}]$_i$, intracellular free Ca^{2+} concentration; EGFP, enhanced GFP; GFP, green fluorescent protein; KRB, Krebs-Ringer buffer; mRFP, monomeric red fluorescent protein; NPY, neuropeptide Y; phogrin, phosphatase on the granule of insulinoma; PPI, preproinsulin; TIRF, total internal reflection fluorescence; Venus, pH-insensitive yellow fluorescent protein.

Type 2 diabetes ultimately results from the failure of insulin secretion from pancreatic β-cells to compensate adequately for peripheral insulin resistance (1–3). While decreases in β-cell mass may contribute (4), the principal failing appears to be abnormal glucose sensing by an extant β-cell mass (1,5,6). The molecular mechanisms involved in glucose-stimulated insulin secretion in the healthy β-cell are increasingly well understood (6). Thus, glucose-induced increases in ATP synthesis, and hence a reduction of free ADP, leads to the closure of ATP-sensitive K^+ channels, cell depolarization, and Ca^{2+} influx through voltage-gated Ca^{2+} channels (6), as well as to the activation of more poorly defined "amplifying" mechanisms (7). However, despite extensive studies in humans (1–3) and the use of rodent models (8,9), understanding of the defects underlying defective insulin secretion in type 2 diabetes is still fragmentary (5).

Imaging techniques represent a powerful tool for detecting vesicle movement and trafficking in live cells and have provided significant advances in understanding the molecular mechanisms of regulated insulin secretion (6,10–19). Thus, we (10,11,16–18,20), and others (12–14,19), have recently developed several approaches to visualize the dynamics of individual insulin release events. These are based on the use of vesicle-targeted forms of green fluorescent protein (GFP) or its enhanced variants in combination with confocal and total internal reflection fluorescence (TIRF) microscopy. Importantly, the latter technique allows fluorescence excitation selectively within a closely restricted domain close to (within 80–150 nm) the plasma membrane (21,22). However, since the targeting of insulin-GFP chimeras to dense-core secretory vesicles has proved problematic (23–25), we have in the past used a relatively pH-insensitive yellow fluorescent protein (Venus) (26) or monomeric red fluorescent protein (mRFP) fused with neuropeptide Y (NPY-Venus or NPY-mRFP, respectively) (16–18) as insulin surrogates in clonal β-cells.

In the present study, we confirm first that NPY provides a more reliable targeting molecule for delivering recombinant fluorescent reporter molecules to the dense-core vesicle than preproinsulin. Through the combined imaging of NPY-mRFP with the vesicle marker phosphatase-on-the-granule-of-insulinoma–enhanced GFP (phogrin-EGFP), we demonstrate next that the majority of exocytosis occurs in primary rat β-cells by transient "cavity recap-

ture" (cavicapture) (17,27) exocytosis rather than complete fusion, in line with previous studies in clonal β-cells (18). We also demonstrate that chronic exposure to elevated glucose concentrations reduces both the number of vesicles that are morphologically docked at the plasma membrane and, unexpectedly, the probability that a single exocytotic event will fully discharge its soluble vesicle cargo. An attenuation of glucose-induced increases in mitochondrial oxidative metabolism, and blunted increases in intracellular Ca^{2+} concentrations ($[Ca^{2+}]_i$), appear likely to underlie the observed abnormalities in the mechanics of single-vesicle fusion.

RESEARCH DESIGN AND METHODS

Expression vectors and adenovirus generation. Plasmids encoding phogrin-EGFP, NPY-mRFP, NPY-Venus (10,16,26), and phogrin-EGFP adenovirus (20) were as described previously. NPY-Venus– and NPY-Y–bearing adenoviruses were generated and amplified using the pAdEasy system (28) as described (20,29). Briefly, cDNAs encoding NPY-Venus or NPY-mRFP were transferred into plasmid pShuttle–cytomegalovirus as *Bgl*II/*Not*I fragments, followed by adenoviral generation from the recombinant shuttle vectors in HEK293 cells.

Isolation and culture of rats islets and MIN6 and INS-1 cell culture. Islets from rats (male Wistar) were isolated by intraductal collagenase digestion and purified on a Histopaque (Sigma, Poole, Dorset, U.K.) gradient (30). For islet dissociation, incubations were performed for 5 min in Ca^{2+}-free solution (138 mmol/l NaCl, 5.6 mmol/l KCl, 1.2 mmol/l $MgCl_2$, 5 mmol/l HEPES, 1 mmol/l EGTA, containing 100 IU/ml penicillin, and 100 mg/ml streptomycin, pH 7.35). After brief centrifugation, the above solution was replaced with RPMI-1640 medium (Life Sciences, Paisley, U.K.) containing 10 mmol/l glucose, 2 mmol/l glutamine, 10% heat-inactivated fetal bovine serum, 100 IU/ml penicillin, and 100 mg/ml streptomycin, and islets were dissociated by gentle pipetting trough a pipette. The released cells were plated on glass coverslips and cultured at 37°C in RPMI-1640 medium containing 10 mmol/l (control) or 30 mmol/l (high glucose) glucose. In the case of high-glucose recovery islets, the medium was changed to RPMI-1640 containing 10 mmol/l glucose after 2 days' culture, and cells were cultured for a further 24 h. MIN6 cells (passage nos. 19–30) and INS-1 cells (passage nos. 100–130) were continuously cultured as described (16,20).

TIRF microscopy. MIN6 cells (16) or dissociated rat islets were plated on to poly-L-lysine–coated high refractive index coverslips (n = 1.78) or bare coverslips (n = 1.53), respectively. Clonal and primary cells were transfected, respectively, with 0.5 or 5 μg plasmids using lipofectAMINE 2000 (Invitrogen), 16 h before imaging. Alternatively, 1 day before imaging, cells were infected with appropriate adenoviruses at a multiplicity of infection of 30 for 4 h (31). Cells were preincubated for 20 min in modified Krebs-Ringer buffer (KRB) containing 125 mmol/l NaCl, 3.5 mmol/l KCl, 1.5 mmol/l $CaCl_2$, 0.5 mmol/l NaH_2PO_4, 0.5 mmol/l $MgSO_4$, 3 mmol/l glucose, 10 mmol/l HEPES, and 2 mmol/l $NaHCO_3$, pH 7.4, and equilibrated with O_2/CO_2 (95:5) and supplemented with 0.1% (wt/vol) BSA. Cells were perifused at 37°C in the same medium during imaging. Stimulation with KCl was achieved by perfusion of 50 mmol/l KCl containing KRB (NaCl was reduced to maintain the osmolarity). β-Cells are likely to represent 60–80% of the cells in preparations used here and were further selected by identifying by eye the largest cells within the field.

A TIRF microscope similar to that described previously (18) was used in conjunction with objective lens, having a numerical aperture of either 1.65 (APO 100×/1.65 HR; Olympus) (22,32) or 1.45 (PlanAPO 100×/1.45 TIRFM; Olympus) for experiments in clonal or primary β-cells, respectively. To analyze the data, fusion events were manually selected, and the average fluorescence intensity of individual granules in a 1 μm × 1 μm square placed over the granule center was calculated. Vesicle movement was quantified using MetaMorph software (Universal Imaging, West Chester, PA), and diffusion coefficients were calculated as described (16).

Confocal imaging. Imaging was performed with a Leica TCS-AOBS laser-scanning confocal microscope (×100 objective), monitoring the bottom of the cell before moving up the confocal plane in 1-μm steps.

Free Ca^{2+} concentration measurements. Dissociated rat islet cells were loaded with 2 μmol/l fura-2-acetoxymethylester (Sigma) for 20 min at 37°C in KRB containing 3 mmol/l glucose. Cells were then transferred into a thermostatted (37°C) chamber mounted on the stage of an inverted microscope used in the epifluorescence mode with a ×40 objective (UAPO/340 40×/1.35; Olympus). Cells were alternately excited at 340 and 380 nm at 5-s intervals using a monochromator (Polychrome IV; Tillphotonics), and emission signals were detected at 515 nm with a cooled charge-coupled device camera with background correction.

NADPH measurements. Reduced pyridine nucleotide fluorescence (NADPH) was excited at 360 nm, and the fluorescence emitted was filtered at 460 nm using the setup above.

Insulin secretion. Islets were preincubated in KRB medium containing 3 mmol/l glucose for 20 min at 37°C and then incubated in KRB medium containing either 3 or 20 mmol/l glucose or 50 mmol/l KCl. Incubations were performed for 20 min at 37°C. Total insulin was extracted in acidified ethanol (29). Insulin was measured using radioimmunoassay by competition with ^{125}I-labeled rat insulin (Linco Research, St. Charles, MO).

Real-time quantitative RT-PCR. Total RNA was extracted from ~100 islets using TRIzol (Invitrogen, Paisley, U.K.). RNA samples were treated with DNA free (Ambion, Austin, TX), and RNA concentration was determined using RiboGreen assay (Molecular Probes, Eugene, OR). Complementary DNA was synthesized from 1 μg total RNA using 2.5 μmol/l random-hexamer primers and murine moloney leukemia virus reverse transcriptase (2.5 units/μl) in buffer containing 5 mmol/l $MgCl_2$ and 1 mmol/l dNTP (Applied Biosystems, Warrington, U.K.). Real-time PCR was performed using 25 ng of reverse-transcribed total RNA with 300 nmol/l of sense and antisense primers, 100 nmol/l dual-labeled probe, 4.0 mmol/l $MgCl_2$, 300 mmol/l dNTP, and 1.25 units HotStar Taq Polymerase (Qiagen, Crawley, U.K.) in a total volume of 25 μl in a DNA Engine Opticon-2 Real-Time PCR Detection System (MJ Research, Waltham, MA). All primer and probe sequences are described in (33) with the exception of Synaptotagmin V (NM_016908; referred to as Syt IX by Fukuda et al. [34]): forward, 5′-GGAAATGTTTCCGACTTCCA-3′; reverse, 5′-GGCTTC ACAGCTGATTGTCA-3′; and probe, 5′-FAM-AAGTCTGGCATCCCCTGCCC TAMRA-3′). Standard curves were constructed by amplifying serial dilutions of untreated islet cDNA (50 ng to 0.64 pg) and plotting cycle threshold (C_T) values.

Data analysis and statistics. Data are given as means ± SE for 10 cells (TIRF imaging), 23–28 clusters of cells [intracellular free Ca^{2+} concentration ($[Ca^{2+}]_i$) and NADPH], or 20 coverslips (insulin secretion) from six different cultures. Statistical significance was assessed by ANOVA followed by a Newman-Keuls test with GraphPad Prism software (GraphPad Software, San Diego, CA).

RESULTS

Visualization of insulin secretion with preproinsulin-EGFP or NPY-Venus. To compare the utility of a range of dense-core vesicle–targeted probes as surrogates for endogenous insulin, we first generated several preproinsulin (PPI)-EGFP constructs (online appendix [available at http://diabetes.diabetejournals.org]). These contained several different lengths of linker sequence between PPI and EGFP or had an inserted Kozak sequence upstream of PPI (online appendix Fig. 1). The targeting efficiency of these PPI-EGFP variants was compared with NPY-Venus by immunocytochemical analysis of fixed cells (online appendix Fig. 2). Examined in either clonal β-cell lines or in primary rat islet cells, the targeting efficiency of PPI-EGFP to vesicles was significantly lower than that of NPY-Venus (online appendix Table 1 and Fig. 2), despite the generation of full-length PPI-EGFP chimeras in each case (online appendix Fig. 2*J*).

We next analyzed the behavior of single PPI-EGFP–expressing vesicles near the plasma membrane in MIN6 cells and rat islet cells by TIRF microscopy (16–18,20,35). We first counted the number of plasma membrane–associated fluorescent vesicles in MIN6 cells under unstimulated conditions. No significant difference was apparent in the number or diameter of plasma membrane–docked vesicles reported with in PPI-EGFP–transfected (1.3 ± 0.2 vesicles/μm^2, n = 7) versus NPY-Venus–transfected (1.2 ± 0.4 vesicles/μm^2, n = 7) or NPY-mRFP–transfected (1.4 ± 0.3 vesicles/μm^2, n = 7) MIN6 cells. These values are similar to electron microscopic observations (36).

To further examine whether NPY-targeted constructs were likely to faithfully report the behavior of vesicular insulin during individual release events, the dynamics of single-vesicle fusion and exocytosis were determined in

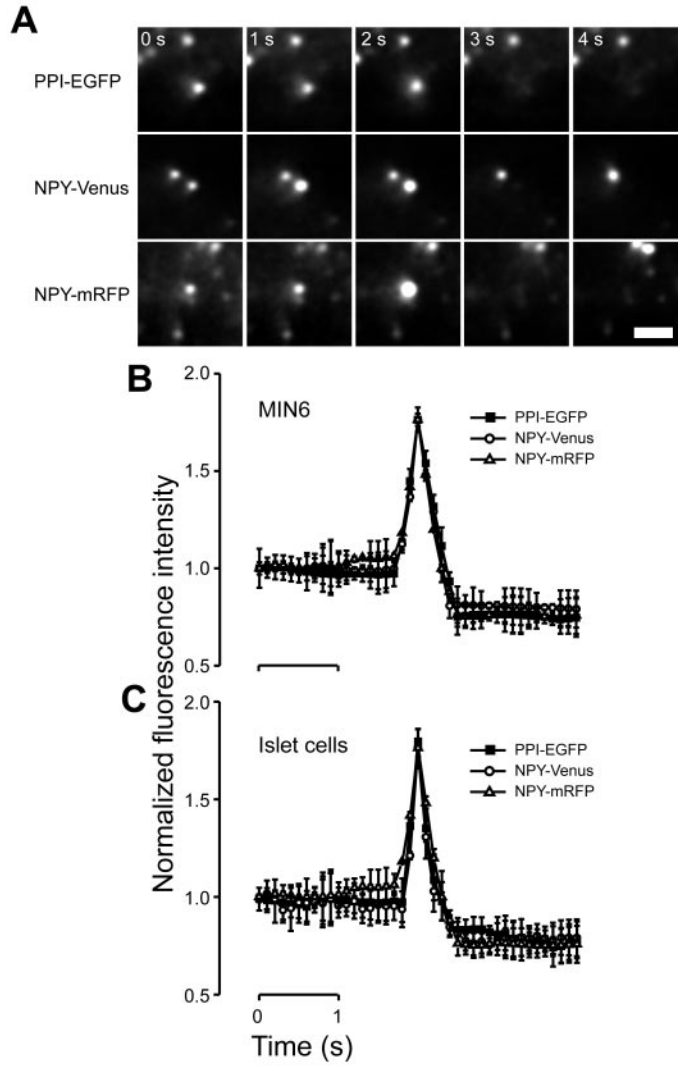

FIG. 1. Fluorescence intensity changes in single PPI-EGFP, NPY-Venus, or NPY-mRFP-expressing vesicle. *A*: Sequential images of a single PPI-EGFP (*top*)-, NPY-Venus (*middle*)-, or NPY-mRFP (*bottom*)-expressing MIN6 cells observed after high KCl stimulation. Scale bar = 2 μm. *B* and *C*: Time course of the fluorescence changes measured in PPI-EGFP (■)-, NPY-Venus (○)-, and NPY-mRFP (△)-expressing MIN6 cells (*B*) and dissociated rat islet cells (*C*). The average fluorescence intensity before fusion was taken as 100% (n = 5 cells in each case). Images were acquired every 100 ms in each condition.

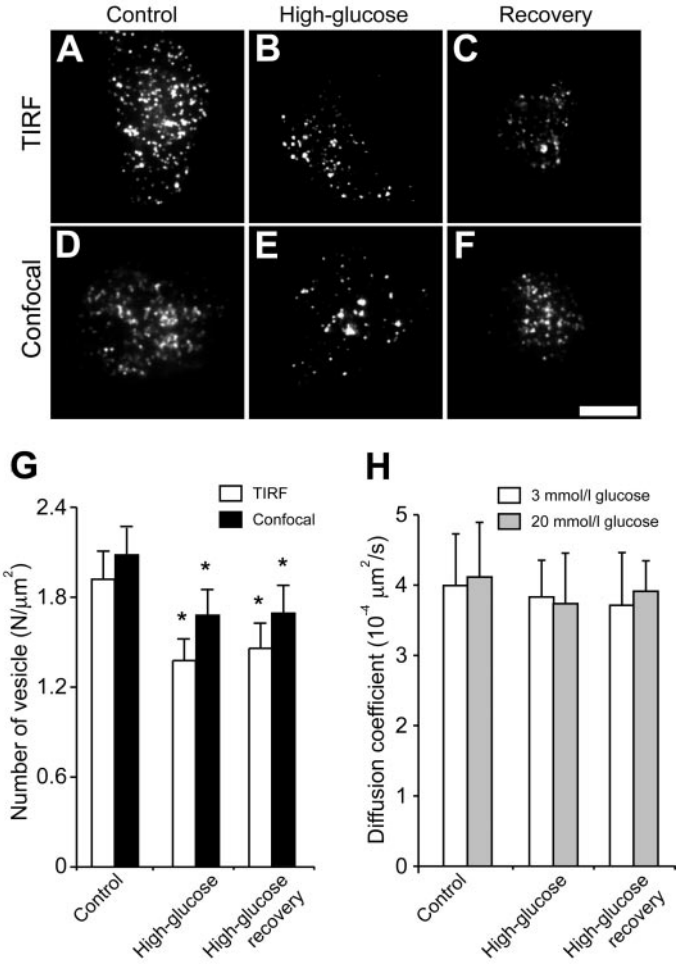

FIG. 2. Effect of hyperglycemia on the number of insulin vesicles docked at the plasma membrane in rat dissociated islets. *A–C*: Typical TIRF images of plasma membrane–docked vesicles observed at 3 mmol/l glucose in control (*A*), high-glucose (*B*), and high-glucose recovery (*C*) dissociated islets. *D–F*: Typical confocal microscopy images of cytosolic vesicles observed at 3 mmol/l glucose in control (*D*), high-glucose (*E*), and high-glucose recovery (*F*) dissociated islets. Scale bars = 5 μm. *G*: The density of docked vesicles was determined by counting the vesicles in each image (100 μm² area, n = 10 cells in each). *P < 0.05 when compared with control. *H*: Mean diffusion coefficients were calculated from vesicle traces obtained using the TIRF microscope (40 vesicles from five cells were analyzed).

PPI-EGFP–, NPY-Venus–, or NPY-mRFP–expressing cells. The release kinetics of PPI-EGFP, NPY-Venus, and NPY-mRFP were essentially identical (Fig. 1*A*). Thus, stimulation with 50 mmol/l KCl caused PPI-EGFP–, NPY-Venus–, or NPY-mRFP–containing spots to brighten and spread suddenly during the release of the fluorescent peptide (16,18), with an identical time course for all three constructs in both clonal MIN6 cells and dissociated rat islet cells (Fig. 1*B* and *C*). Furthermore, overexpression of PPI-EGFP, NPY-Venus, or NPY-mRFP had no significant inhibitory effect on the release of endogenous insulin (data not shown). These data confirm the more efficient routing of NPY- than PPI-based chimeras to dense-core vesicles.

Sustained exposure to high glucose concentrations decreases the number of docked vesicles on the plasma membrane. We next determined the effects of culturing islets under severely hyperglycemic conditions (high glucose: 30 mmol/l glucose) compared with culture under the mildly hyperglycemic conditions (control: 10 mmol/l glucose) previously shown to be optimal for the survival and the preservation function of rat islets (37) and isolated β-cells (38) ex vivo. Note that culture at lower glucose concentrations (5–7 mmol/l) (39) decreases both insulin content and glucose-induced insulin secretion from isolated β-cells and islets (38,40), while prompting apoptosis (41), and was not, therefore, used here.

To determine whether high-glucose treatment might inhibit vesicle transport or docking at the plasma membrane, we counted the number of plasma membrane–associated and intracellular vesicles labeled with NPY-Venus by TIRF (Fig. 2*A–C*) or confocal microscopy (Fig. 2*D–F*), respectively. Cells cultured at 30 mmol/l displayed a significantly reduced number of both intracellular and plasma membrane–docked vesicles (Fig. 2*B*, *E*, and *G*) compared with control cells maintained at 10 mmol/l glucose. These effects were largely unaltered by subsequent culture for a further 24 h at 10 mmol/l glucose (high-glucose recovery; Fig. 2*C*, *F*, and *G*).

We next determined whether culture at 30 mmol/l

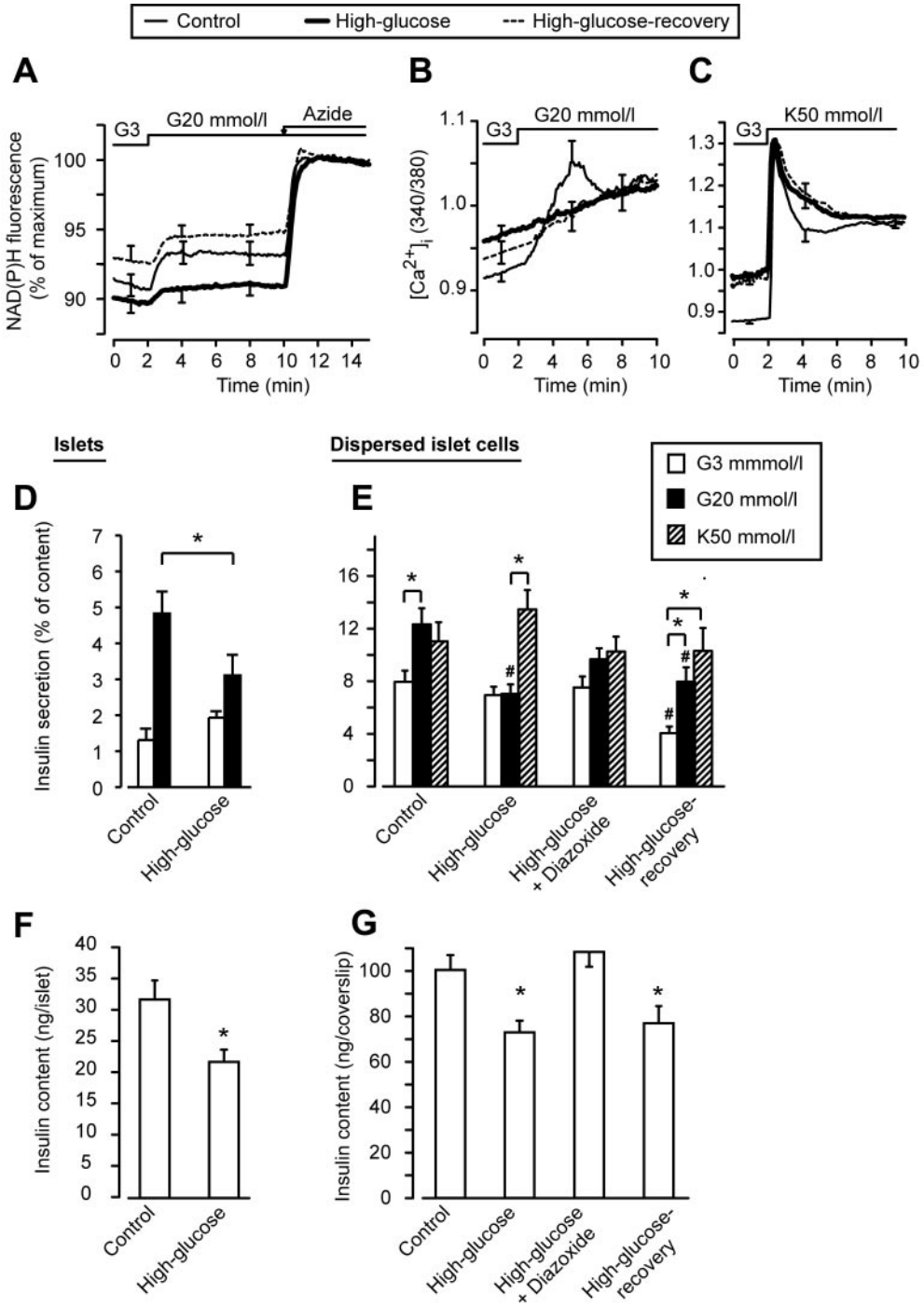

FIG. 3. Glucose-induced changes in metabolism, $[Ca^{2+}]_i$, and insulin secretion. *A–C*: Dispersed islet cells were perifused for 20 min with a medium containing 3 mmol/l glucose and were stimulated with either 20 mmol/l glucose or high KCl, as indicated. Changes in NADPH fluorescence are shown as percentages of mean fluorescent levels measured from 12 to 13 min after addition of 2 mmol/l sodium azide (*A*). Changes of $[Ca^{2+}]_i$ are expressed as ratiometric (340/380) changes (*B* and *C*). Note that the apparent slow increase in $[Ca^{2+}]_i$ as reported by the 340/380 fluorescence ratio in *B* is likely to be due to the slow leakage of fura-2 from the cells in these experiments. *D* and *E*: Insulin secretion is expressed as a percentage of total insulin content. #$P < 0.05$ vs. control in 3 mmol/l glucose. *F* and *G*: Insulin content of islets and dispersed islet cells.

glucose inhibited vesicle movement subsequently stimulated by 20 mmol/l glucose. Control, high-glucose, and high-glucose recovery islet cells were imaged by TIRF microscopy to analyze vesicle movement beneath the plasma membrane (Fig. 2*H*) (16). The diffusion coefficient value in 20 mmol/l glucose-stimulated control islets was $4.1 \pm 0.87 \times 10^{-4}$ $\mu m^2/s$ ($n = 12$ cells), similar to values for adrenal chromaffin (42) and MIN6 β-cells (16). High-glucose treatment did not alter basal or 20 mmol/l glucose-induced vesicle movement (Fig. 2*H*, high glucose and high-glucose recovery).

Elevated glucose concentrations inhibit mitochondrial oxidative metabolism, $[Ca^{2+}]_i$ increases, and insulin secretion in response to subsequent challenge with glucose. To determine the effects of elevated culture glucose concentrations on the subsequent metabolic responses to acute stimulation with the sugar, we monitored glucose-induced changes in reduced pyridine nucleotide fluorescence and $[Ca^{2+}]_i$. Increasing glucose from 3 to 20 mmol/l induced a significantly smaller elevation in NADPH autofluorescence in high-glucose–treated as in control islet cells (0.95 ± 0.31 vs. 2.21 ± 0.31%, respectively, $P < 0.05$; Fig. 3*A*). The abnormal response observed in high-glucose cells was partially corrected by culture with 10 mmol/l glucose for a further 24 h (1.64 ± 0.49%; high-glucose recovery; Fig. 3*A*).

Compared with control cells, resting $[Ca^{2+}]_i$, measured at 3 mmol/l glucose, was higher in high-glucose or high-

glucose recovery islet cells (Fig. 3*B* and *C*) in line with previous reports in rat and human islets (37,43,44). Moreover, further increases in $[Ca^{2+}]_i$ upon stimulation with 20 mmol/l glucose were markedly attenuated in cells incubated at 30 mmol/l (0.035 ± 0.003 vs. 0.089 ± 0.014 fluorescence ratio units, $P < 0.001$), an effect partially reversed by culture for a further 24 h at 10 mmol/l glucose (0.052 ± 0.007, $P < 0.01$ vs. control and $P < 0.05$ vs. high glucose; Fig. 3*B*). In contrast, the increase in $[Ca^{2+}]_i$ in response to 50 mmol/l KCl was unaltered in high-glucose–treated cells (Fig. 3*C*).

The above results indicated that high-glucose treatment lessened the augmentation of mitochondrial metabolism in response to a step increase in glucose concentration, consequently decreasing Ca^{2+} influx. In line with this, compared with control islets, insulin secretion from high-glucose–treated islet or dispersed islets cells was significantly lower at 20 mmol/l glucose (Fig. 3*D* and *E*). Glucose-induced insulin secretion was partially restored in cells treated either with 100 μmol/l diazoxide (to inhibit insulin release) or with 10 mmol/l glucose for a further 24 h (high-glucose recovery, Fig. 3*E*). Again, insulin secretion in response to 50 mmol/l KCl was unaffected by high-glucose treatment (Fig. 3*E*).

In line with the reduced number of intracellular and plasma membrane–docked vesicles (Fig. 2), total insulin content was ~30% lower in high-glucose than in control cells (Fig. 3*F* and *G*). This defect was corrected by culturing cells in the presence of diazoxide but not by lowering the glucose concentration to 10 mmol/l for a further 24 h (Fig. 3*G*).

Suggesting that the alterations in glucose-induced NADPH changes and $[Ca^{2+}]$ may be due to changes in the expression of genes involved in glucose sensing, quantitative PCR revealed decreases in the levels of mRNAs encoding Glut2 and glucokinase in cultured intact islets (Fig. 4*A* and *B*), and a tendency toward decreased expression in dissociated islets (Fig. 4*D* and *E*), after culture under high-glucose conditions. These changes were fully reversible upon further culture at 10 mmol/l glucose. In addition, culture at 30 vs. 10 mmol/l glucose caused a small but significant decrease in the level of mRNA encoding the exocytotic Ca^{2+} sensor synaptotagmin V /synaptotagmin IX (34) in intact (Fig. 4*C*) but not dissociated (Fig. 4*F*) islets.

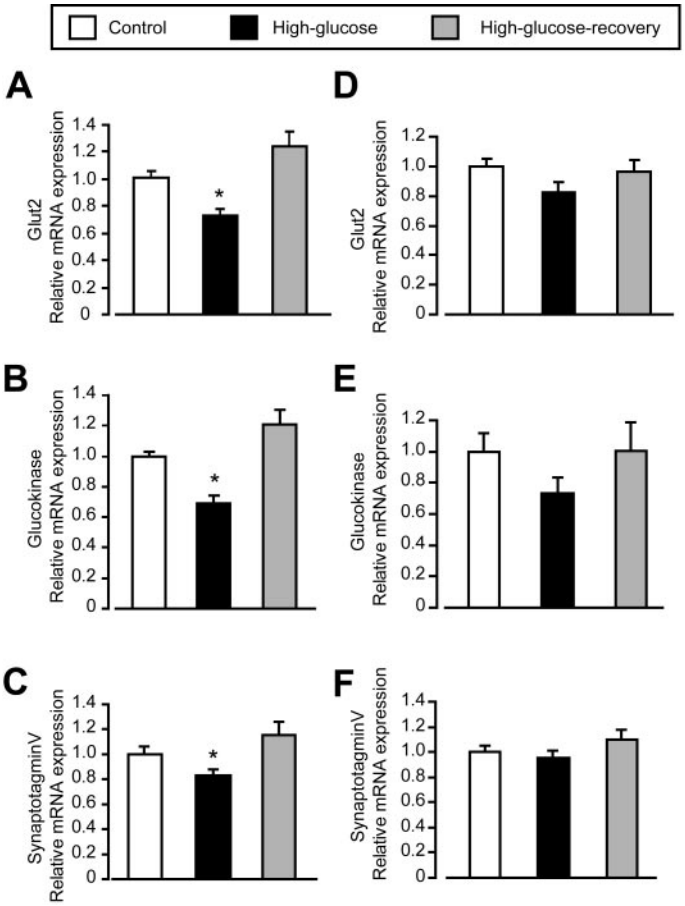

FIG. 4. High-glucose culture reduces Glut2, glucokinase, and synaptotagmin V mRNA expression in islets. Islets were cultured either as whole islets in suspension (*A–C*) or dispersed in islet cells (*D–F*). mRNA levels of the indicated genes were analyzed by quantitative real-time RT-PCR. Results are expressed as fold changes over control.

Effects of elevated glucose concentrations on the mechanics of vesicle fusion. We recently demonstrated using the vesicle cargo protein NPY-Venus (18) and lower molecular mass molecules (20) that insulin release is likely to occur via transient kiss-and-run or cavity recapture (cavicapture) exocytosis (17,27). The kinetics of release were shown in these earlier studies to be dependent upon the magnitude of the imposed increase in $[Ca^{2+}]_i$ (17). To determine whether exocytosis occurred via similar mechanisms in primary rat β-cells, we coinfected control, high-glucose, and high-glucose recovery islet cells with adenoviruses expressing phogrin-EGFP and NPY-mRFP. Individual exocytotic events were then studied with a dual-color TIRF microscope. Examined in control cells, stimulation with 20 mmol/l glucose may cause the near-complete release of NPY-mRFP fluorescence from vesicles (Fig. 5*A*; Fig. 6*A* and *D*, *trace A*). In contrast, phogrin-EGFP fluorescence in the same vesicles diminished only slightly (Fig. 5*A*), as observed in clonal INS-1 and MIN6 cells (18,20). Examined in several similar experiments, the majority of the NPY-mRFP fluorescence was lost rapidly from the vesicles (Fig. 5*B*, ■). By contrast, phogrin-EGFP fluorescence remained nearly constant (Fig. 5*B*, ○), arguing against complete vesicle collapse into the plasma membrane after individual secretory events.

To determine whether high-glucose treatment altered the kinetics of single-fusion events or the extent of the fusion process, similar experiments were performed using high-glucose and high-glucose recovery cells (Fig. 5*C* and *E*). In all cases, the kinetics of the increase and decrease in NPY-mRFP fluorescence were similar (Fig. 5*A–F*). Moreover, vesicular phogrin-EGFP remained associated with the vesicle and failed to spread into the plasma membrane after exocytosis of NPY-mRFP, consistent with a cavicapture mechanism, in each case.

We next determined whether culture at high glucose affected the nature of the release events by quantifying the extent of cargo (NPY-Venus) release. Glucose (20 mmol/l) stimulation caused either the apparent release of NPY-Venus, as monitored through a transient increase in fluorescence followed by diffusion away from the site of exocytosis (Fig. 6*A* and *D*), as previously reported in MIN6 β-cells (17,18), or little decrease in NPY-Venus fluorescence, compared with the preevent level apparent after the termination of the event (Fig. 6*B* and *C*). Compared with control cells, high-glucose–treated cells showed a significant decrease of the number of full-release events for NPY-Venus in response to

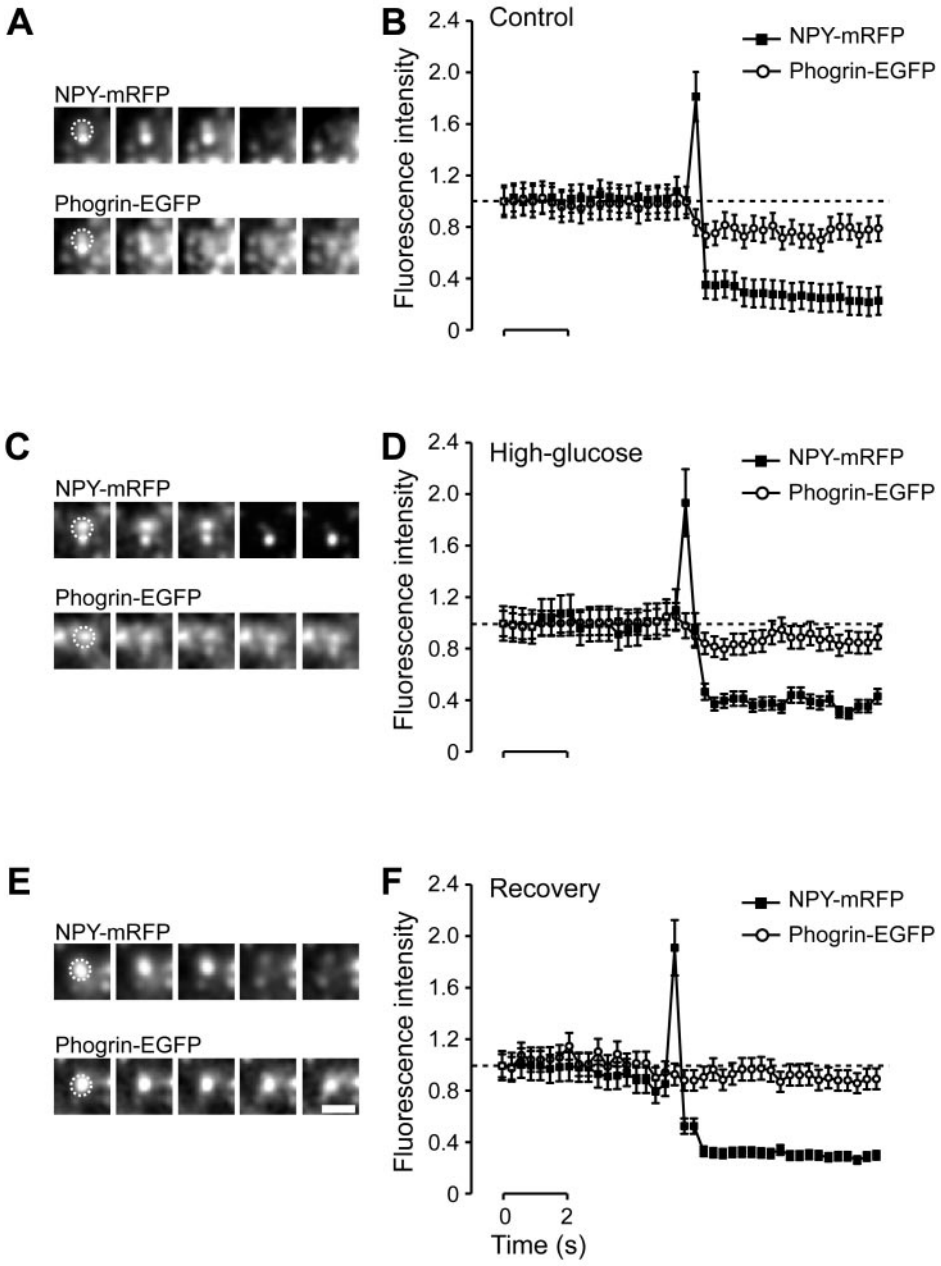

FIG. 5. Phogrin remains on the secretory vesicle after exocytosis. Five sequential dual-color TIRF images show the behavior of single phogrin-EGFP and NPY-mRFP in control (*A*), high-glucose (*C*), and high-glucose recovery (*E*) vesicles after applying 20 mmol/l glucose. The position before exocytosis is outlined by a circle. Image were acquired every 300 ms. Scale bar = 1 μm. Average fluorescence intensity traces are from control (*B*), high-glucose (*D*), and high-glucose recovery (*F*) dissociated islets.

20 mmol/l glucose (Fig. 6*E* and *F*), which was reversed by incubation with 10 mmol/l glucose for a further 24 h (Fig. 6*E* and *F*). These results indicate that a decrease in the number of complete-fusion events, i.e., those leading to complete release of the vesicle's cargo of insulin rather than a reduction in the total number of events, is largely responsible for the decrease in insulin output from cells or islets treated under high-glucose conditions. By contrast, the number and type of release events were similar in response to 50 mmol/l KCl, under all culture conditions (Fig. 6*E* and *F*).

DISCUSSION

Targeting of recombinant fluorescent reporters to dense-core vesicles in pancreatic β-cells. The first aim of the present study was to reassess the targeting efficiency of PPI- versus NPY-based constructs in clonal β-cells and in primary islet cells. After fusion with PPI, targeting of fluorescent proteins to secretory vesicles was relatively poor in insulinoma cell lines (<60%) though higher than we described previously for PPI-GFP (23), a construct that lacked a linker sequence. The most likely explanation for the low targeting efficiency of both PPI-GFP and PPI-EGFP in clonal β-cells is misfolding of the (pro)insulin or EGFP moieties and consequent retention in the endoplasmic reticulum or missorting in the *trans*-Golgi network (45). Of note, the targeting efficiency to granules was higher for each of the PPI-EGFP constructs when assessed in primary, rather than in clonal, β-cells, in line with the more efficient sorting of endogenous insulin to the regulated secretory pathway in the former setting (45). Nevertheless, in each of the cell types examined, NPY-based chimeras displayed more efficient targeting to dense-core vesicles than those based on PPI, presumably reflecting the less rigorous demands for folding and sorting to vesicles of the smaller NPY peptide. NPY-based constructs were therefore used in subsequent studies as convenient surrogates for endogenous insulin.

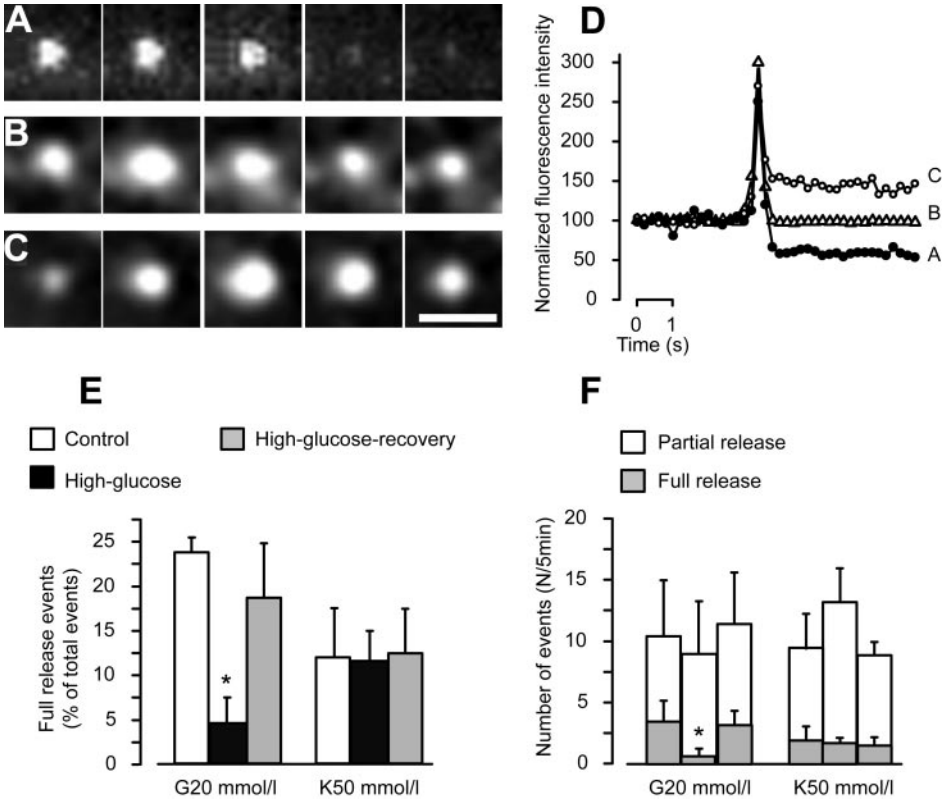

FIG. 6. Effect of hyperglycemia on the kinetics of NPY-Venus release. *A–C*: Typical sequential images of full (*A*) and partial (*B* and *C*) NPY-Venus release events observed after 20 mmol/l glucose-stimulated control dissociated islets under the TIRF microscope. Images were acquired every 200 ms in each condition. Scale bar = 1 μm. *D*: Time course of the fluorescence changes measure in the center of NPY-Venus vesicles shown in *A* (■), *B* (△), and *C* (○). *E*: The percentage of full-release events was calculated in control, high-glucose, and high-glucose recovery dispersed islet cells during 20 mmol/l glucose or 50 mmol/l KCl stimulation, as indicated. *F*: Numbers of fusion events were counted per cell in the same cell population as in *E*.

Insulin secretion occurs by a transient, cavicapture mechanism in primary rat islet β-cells. The second aim of the present study was to reassess the mechanics of individual release events in the context of primary rodent β-cells. While we have previously reported that release of insulin occurs principally via a cavity recapture process in clonal β-cells (17,18), recent data obtained using two-photon, confocal, and TIRF microscopy of pancreatic islets indicated that stimulation in the presence of fluorescent tracer resulted in the abrupt appearance of small "omega" shape fluorescent spots at the plasma membrane and then rapidly disappeared (12,15). It was therefore concluded that the majority of insulin exocytosis involved full fusion of the vesicle and plasma membranes. However, in neither of these studies was the fate of a secretory vesicle membrane protein (e.g., phogrin) monitored. By contrast, in the present work, simultaneous observation of phogrin-EGFP and NPY-mRFP revealed that only a small decrease in phogrin-EGFP fluorescence, with no spreading into the plasma membrane as would be predicted for a full fusion event, occurred at the time of the NPY-mRFP release in rat islet cells. The most straightforward interpretation of these data are that the majority of exocytosis occurs via transient "cavicapture" exocytosis in primary islet cells, as observed in clonal β-cells (17,18) and other neuroendocrine cells (46).

Impact of sustained high glucose concentrations on the kinetics of individual exocytotic events. The present studies demonstrate that, after culture of rat islet cells at 30 (vs. 10) mmol/l glucose, partial or incomplete release of vesicle content frequently occurred. What may be the underlying mechanisms? We have previously reported that in MIN6 cells, the mode of exocytosis is dependent upon the strength of stimulation, with a progressive shift from very transient (pure kiss and run) to more sustained events, involving the opening of a larger fusion pore (quasi full fusion) (17), as Ca^{2+} concentrations increase. Thus, abnormal Ca^{2+} signaling would be expected to lead to a decrease in the number of these more sustained opening events (17), which are necessary to allow release of insulin monomers (18).

Correspondingly, we show here that long-term exposure to high glucose induces marked abnormalities in the regulation of $[Ca^{2+}]_i$ in dissociated rat islet cells, with both a small increase in basal $[Ca^{2+}]_i$ and a marked attenuation of glucose-induced $[Ca^{2+}]_i$ increases, assuming similar behavior of fura-2 under all conditions. The data are broadly consistent with those previously obtained with mouse (47), rat (37), and human (37,43) islets cultured under hyperglycemic conditions. Similarly, our finding that secretion stimulated by 20 vs. 3 mmol/l glucose was slightly or completely attenuated by high-glucose culture of intact (Fig. 3*D*) or dispersed (Fig. 3*E*) islets, respectively, is in line with the findings of Khaldi et al. (37) but in slight contrast to the results of Ling et al. (38), where different culture and stimulation protocols were used.

The abnormalities in glucose-induced Ca^{2+} signaling described here seem likely to be due, at least in part, to a perturbation in the normal stimulation by glucose of mitochondrial oxidative metabolism, given the smaller glucose-induced increases in mitochondrial pyridine nucleotide fluorescence observed after chronic hyperglycemia. Importantly, the alterations in glucose metabolism and Ca^{2+} homeostasis, and the changes in the mechanics of single insulin release events, were at least partially reversible upon the return of glucose to optimal levels. While the mechanisms involved remain to be elucidated, reversible changes in the expression of key genes involved in glucose sensing, including Glut2 and glucokinase (Fig. 4) as well as uncoupling protein 2 (31), seem more likely to be involved than irreversible β-cell damage or apoptosis ("glucotoxicity") (48).

Finally, downstream changes in the expression of Ca^{2+}-sensing proteins, such as synaptotagmin V (Fig. 4*C* and *F*), may also amplify the effects of defective glucose metabolism and Ca^{2+} signaling to further weaken the exocytotic response to glucose. Importantly, decreases in the expression of SytV, a positive regulator of exocytosis, in the face of unaltered expression of dynamin-1 (data not shown), involved in the termination of the exocytotic event (18), may contribute to the observed decrease in the number of complete exocytotic events that lead to the efficient release of insulin (Fig. 6*F*).

In conclusion, by combining the targeting of NPY-based fluorescent probes to dense-core secretory vesicles with confocal and TIRF microscopy, we describe for the first time the nanomechanics of individual exocytotic events in the physiological setting of primary rat β-cells. We show that elevated glucose concentrations lead to defects in glucose signaling and abnormal termination of exocytotic events, resulting in the inhibition of glucose-induced insulin secretion. Such phenomena may therefore contribute to defective insulin secretion in some forms of type 2 diabetes.

ACKNOWLEDGMENTS

This work was supported by grants from the Wellcome Trust (to G.A.R.; project 062321, program 067081/Z/02/Z), the Juvenile Diabetes Research Foundation International (JDRFI; 1-2003-235), the Biotechnology and Biological Sciences Research Council, the Human Frontiers Science Program, and Diabetes U.K. T.T. thanks the JDRFI for a Postdoctoral Fellowship, and G.A.R thanks the Wellcome Trust for a Research Leave Fellowship.

We are grateful to Dr. Mark Jepson and Alan Leard of the Bristol MRC Cell Imaging Facility for technical support. We thank Katsuyuki Abe (Olympus Optical, Tokyo, Japan) and Hitoshi Hatano (Olympus UK Lt, Middlesex, U.K.) for generous technical support; Drs. Graeme I. Bell, Atsushi Miyawaki, and Roger Y. Tsien for plasmids; and Rebecca Rowe for isolation and preparation of islets culture.

REFERENCES

1. Chiasson JL, Rabasa-Lhoret R: Prevention of type 2 diabetes: insulin resistance and β-cell function. *Diabetes* 53 (Suppl. 3):S34–S38, 2004
2. DeFronzo RA: Pathogenesis of type 2 (non-insulin dependent) diabetes mellitus: a balanced overview. *Diabetologia* 35:389–397, 1992
3. Stumvoll M: Minkowski Lecture 2003: Control of glycaemia: from molecules to men. *Diabetologia* 47:770–781, 2004
4. Butler AE, Janson J, Soeller WC, Butler PC: Increased β-cell apoptosis prevents adaptive increase in β-cell mass in mouse model of type 2 diabetes: evidence for role of islet amyloid formation rather than direct action of amyloid. *Diabetes* 52:2304–2314, 2003
5. Ashcroft FM, Rorsman P: Molecular defects in insulin secretion in type-2 diabetes. *Rev Endocr Metab Disord* 5:135–142, 2004
6. Rutter GA: Minkowski Lecture 2004: Visualising insulin secretion. *Diabetologia* 47:1861–1872, 2004
7. Henquin JC: Triggering and amplifying pathways of regulation of insulin secretion by glucose. *Diabetes* 49:1751–1760, 2000
8. Tokuyama Y, Sturis J, DePaoli AM, Takeda J, Stoffel M, Tang J, Sun X, Polonsky KS, Bell GI: Evolution of β-cell dysfunction in the male Zucker diabetic fatty rat. *Diabetes* 44:1447–1457, 1995
9. Gaisano HY, Ostenson CG, Sheu L, Wheeler MB, Efendic S: Abnormal expression of pancreatic islet exocytotic soluble N-ethylmaleimide-sensitive factor attachment protein receptors in Goto-Kakizaki rats is partially restored by phlorizin treatment and accentuated by high glucose treatment. *Endocrinology* 143:4218–4226, 2002
10. Pouli AE, Emmanouilidou E, Zhao C, Wasmeier C, Hutton JC, Rutter GA: Secretory-granule dynamics visualized in vivo with a phogrin-green fluorescent protein chimaera. *Biochem J* 333:193–199, 1998
11. Varadi A, Ainscow EK, Allan VJ, Rutter GA: Involvement of conventional kinesin in glucose-stimulated secretory granule movements and exocytosis in clonal pancreatic beta-cells. *J Cell Sci* 115:4177–4189, 2002
12. Ma L, Bindokas VP, Kuznetsov A, Rhodes C, Hays L, Edwardson JM, Ueda K, Steiner DF, Philipson LH: Direct imaging shows that insulin granule exocytosis occurs by complete vesicle fusion. *Proc Natl Acad Sci U S A* 101:9266–9271, 2004
13. Ohara-Imaizumi M, Nishiwaki C, Kikuta T, Nagai S, Nakamichi Y, Nagamatsu S: TIRF imaging of docking and fusion of single insulin granule motion in primary rat pancreatic beta-cells: different behaviour of granule motion between normal and Goto-Kakizaki diabetic rat beta-cells. *Biochem J* 381:13–18, 2004
14. Ohara-Imaizumi M, Nakamichi Y, Tanaka T, Ishida H, Nagamatsu S: Imaging exocytosis of single insulin secretory granules with evanescent wave microscopy: distinct behavior of granule motion in biphasic insulin release. *J Biol Chem* 277:3805–3808, 2002
15. Takahashi N, Kishimoto T, Nemoto T, Kadowaki T, Kasai H: Fusion pore dynamics and insulin granule exocytosis in the pancreatic islet. *Science* 297:1349–1352, 2002
16. Tsuboi T, daSilvaXavier G, Leclerc I, Rutter GA: 5′-AMP-activated protein kinase controls insulin-containing secretory vesicle dynamics. *J Biol Chem* 278:52042–52051, 2003
17. Tsuboi T, Rutter GA: Multiple forms of "kiss-and-run" exocytosis revealed by evanescent wave microscopy. *Curr Biol* 13:563–567, 2003
18. Tsuboi T, McMahon HT, Rutter GA: Mechanisms of dense core vesicle recapture following "kiss and run" ("cavicapture") exocytosis in insulin-secreting cells. *J Biol Chem* 279:47115–47124, 2004
19. Barg S, Olofsson CS, Schriever-Abeln J, Wendt A, Gebre-Medhin S, Renstrom E, Rorsman P: Delay between fusion pore opening and peptide release from large dense-core vesicles in neuroendocrine cells. *Neuron* 33:287–299, 2002
20. Tsuboi T, Zhao C, Terakawa S, Rutter GA: Simultaneous evanescent wave imaging of insulin vesicle membrane and cargo during a single exocytotic event. *Curr Biol* 10:1307–1310, 2000
21. Axelrod D: Total internal reflection fluorescence microscopy in cell biology. *Traffic* 2:764–774, 2001
22. Terakawa S, Tsuboi T, Sakurai T, Jeromin A, Wakazono Y, Yamamoto S, Abe K: Fluorescence micro-imaging of living cells and biomolecules with ultra high NA objectives. In *Proceedings of SPIE, Vol. 4597*. Chiou AET, Podbielska H, Jacques SL, Eds. Bellingham, WA, SPIE (International Society for Optical Engineering), 2001, p. 121–127
23. Pouli AE, Kennedy HJ, Schofield JG, Rutter GA: Insulin targeting to the regulated secretory pathway after fusion with green fluorescent protein and firefly luciferase. *Biochem J* 331:669–675, 1998
24. Tompkins LS, Clark SA, Gordon DA, Garrivito N, Lynch RM: Targeting GFP to secretory vesicles in an insulin-secreting pancreatic β-cell line (Abstract). *FASEB J* 12:A428, 1998
25. Tompkins LS, Nullmeyer KD, Murphy SM, Weber CS, Lynch RM: Regulation of secretory granule pH in insulin-secreting cells. *Am J Physiol Cell Physiol* 283:C429–C437, 2002
26. Nagai T, Ibata K, Park ES, Kubota M, Mikoshiba K, Miyawaki A: A variant of yellow fluorescent protein with fast and efficient maturation for cell-biological applications. *Nat Biotechnol* 20:87–90, 2002
27. Henkel AW, Almers W: Fast steps in exocytosis and endocytosis studied by capacitance measurements in endocrine cells. *Curr Opin Neurobiol* 6:350–357, 1996
28. He TC, Zhou S, da Costa LT, Yu J, Kinzler KW, Vogelstein B: A simplified system for generating recombinant adenoviruses. *Proc Natl Acad Sci U S A* 95:2509–2514, 1998
29. Ainscow EK, Zhao C, Rutter GA: Acute overexpression of lactate dehydrogenase-A perturbs β-cell mitochondrial metabolism and insulin secretion. *Diabetes* 49:1149–1155, 2000
30. Kennedy HJ, Pouli AE, Ainscow EK, Jouaville LS, Rizzuto R, Rutter GA: Glucose generates sub-plasma membrane ATP microdomains in single islet beta-cells: potential role for strategically located mitochondria. *J Biol Chem* 274:13281–13291, 1999
31. Diraison F, Parton L, Ferre P, Foufelle F, Briscoe CP, Leclerc I, Rutter GA: Over-expression of sterol-regulatory-element-binding protein-1c (SREBP1c) in rat pancreatic islets induces lipogenesis and decreases glucose-stimulated insulin release: modulation by 5-aminoimidazole-4-carboxamide ribonucleoside (AICAR). *Biochem J* 378:769–778, 2004
32. Terakawa S, Sakurai T, Abe K: Development of an objective lens with a high numerical aperture for light microscopy (Review). *Bioimages* 5:24, 1997
33. Parton LE, Diraison F, Neill SE, Ghosh SK, Rubino MA, Bisi JE, Briscoe CP, Rutter GA: Impact of PPAR{gamma} over-expression and activation on

pancreatic islet gene expression profile analysed with oligonucleotide microarrays. *Am J Physiol Endocrinol Metab* 287:E390–E404, 2004
34. Fukuda M, Kanno E, Mikoshiba K: Conserved N-terminal cysteine motif is essential for homo- and heterodimer formation of synaptotagmins III, V, VI, and X. *J Biol Chem* 274:31421–31427, 1999
35. Tsuboi T, Terakawa S, Scalettar BA, Fantus C, Roder J, Jeromin A: Sweeping model of dynamin activity: visualization of coupling between exocytosis and endocytosis under an evanescent wave microscope with green fluorescent proteins. *J Biol Chem* 277:15957–15961, 2002
36. Braun M, Wendt A, Birnir B, Broman J, Eliasson L, Galvanovskis J, Gromada J, Mulder H, Rorsman P: Regulated exocytosis of GABA-containing synaptic-like microvesicles in pancreatic beta-cells. *J Gen Physiol* 123:191–204, 2004
37. Khaldi MZ, Guiot Y, Gilon P, Henquin JC, Jonas JC: Increased glucose sensitivity of both triggering and amplifying pathways of insulin secretion in rat islets cultured for 1 wk in high glucose. *Am J Physiol Endocrinol Metab* 287:E207–E217, 2004
38. Ling Z, Kiekens R, Mahler T, Schuit FC, Pipeleers-Marichal M, Sener A, Klöppel G, Malaisse WJ, Pipeleers DG: Effects of chronically elevated glucose levels on the functional properties of rat pancreatic β-cells. *Diabetes* 45:1774–1782, 1996
39. Pascoe WS, Storlien LH: Inducement by fat feeding of basal hyperglycemia in rats with abnormal beta-cell function: model for study of etiology and pathogenesis of NIDDM. *Diabetes* 39:226–233, 1990
40. Svensson C, Sandler S, Hellerstrom C: Lack of long-term beta-cell glucotoxicity in vitro in pancreatic islets isolated from two mouse strains (C57BL/6J; C57BL/KsJ) with different sensitivities of the beta-cells to hyperglycaemia in vivo. *J Endocrinol* 136:289–296, 1993
41. Van de CM, Kefas BA, Cai Y, Heimberg H, Scott DK, Henquin JC, Pipeleers D, Jonas JC: Prolonged culture in low glucose induces apoptosis of rat pancreatic beta-cells through induction of c-myc. *Biochem Biophys Res Commun* 312:937–944, 2003
42. Steyer JA, Almers W: Tracking single secretory granules in live chromaffin cells by evanescent-field fluorescence microscopy. *Biophys J* 76:2262–2271, 1999
43. Bjorklund A, Lansner A, Grill VE: Glucose-induced $[Ca^{2+}]_i$ abnormalities in human pancreatic islets: important role of overstimulation. *Diabetes* 49:1840–1848, 2000
44. Grill V, Bjorklund A: Overstimulation and β-cell function. *Diabetes* 50 (Suppl. 1):S122–S124, 2001
45. Molinete M, Lilla V, Jain R, Joyce PB, Gorr SU, Ravazzola M, Halban PA: Trafficking of non-regulated secretory proteins in insulin secreting (INS-1) cells. *Diabetologia* 43:1157–1164, 2000
46. Taraska JW, Perrais D, Ohara-Imaizumi M, Nagamatsu S, Almers W: Secretory granules are recaptured largely intact after stimulated exocytosis in cultured endocrine cells. *Proc Natl Acad Sci U S A* 100:2070–2075, 2003
47. Gilon P, Jonas JC, Henquin JC: Culture duration and conditions affect the oscillations of cytoplasmic calcium concentration induced by glucose in mouse pancreatic islets. *Diabetologia* 37:1007–1014, 1994
48. Robertson RP, Harmon J, Tran PO, Poitout V: β-Cell glucose toxicity, lipotoxicity, and chronic oxidative stress in type 2 diabetes. *Diabetes* 53 (Suppl. 1):S119–S124, 2004